

Thermodynamic evidence for novel quantum criticality in a frustrated metal

Shunichiro Kittaka,^{1,*} Yohei Kono,¹ Suguru Tsuda,² Toshiro Takabatake,² and Toshiro Sakakibara¹

¹*Institute for Solid State Physics, University of Tokyo, Kashiwa, Chiba 277-8581, Japan*

²*Department of Quantum matter, AdSM, Hiroshima University, Higashi-Hiroshima 739-8530, Japan*

Various exotic phases of matter have been discovered near a quantum critical point where magnetic order is suppressed to absolute zero temperature by strong quantum fluctuations. There have remained fundamental questions whether geometrical frustration preventing magnetic long-range order can induce quantum critical phenomena and how novel they are. Here, we employ a magnetic field angle as a tuning parameter and provide thermodynamic evidence for novel quantum criticality not only driven but also augmented by frustration in the quasi-kagome Kondo-lattice CeRhSn. The field-angle-resolved landscape of the entropy reveals the existence of a quantum critical line under a magnetic field, exactly parallel to the quasi-kagome plane. In particular, on this line, we observe a two-step decrease of the entropy accompanied by a qualitative change in the non-Fermi-liquid behavior. These results suggest that a partial release of frustration induces a quantum critical “phase”, whose nature is distinctly different from the zero-field one.

The breakdown of the Fermi-liquid (FL) theory is one of major topics in many-body physics.^{1–6} There have been considerable efforts to understand the mechanisms underlying strange metallic behaviors, including exotic superconductivity, by tuning external parameters such as the magnetic field, pressure and chemical doping.^{3–9} Although most of them arise only in the vicinity of a quantum critical point (QCP) where the magnetic order vanishes, astonishing zero-field quantum criticality (QC) without fine-tuning has been discovered recently for several metals.^{10–12} Further experimental realization of such unusual quantum critical phenomena has remained a challenge. For determining how QC develops near a QCP, the entropy landscape provides fundamental information because the ground states become prominently degenerated near the QCP.^{13,14} From this point of view, field-angle-resolved measurements of entropy, which have been developed recently by taking advantage of the rotational magnetocaloric effect,¹⁵ are powerful for unraveling the mechanism of QC in anisotropic systems.

In this study, we focus on CeRhSn which is categorized as a new class of novel metals that show zero-field QC driven by geometrical frustration.¹⁶ CeRhSn has a hexagonal ZrNiAl-type structure with space group $P\bar{6}2m$, in which basal layers are stacked alternately along the c axis and the Ce sublattice can be viewed as a quasi-kagome lattice (inset of Fig. 2a); it is isostructural with e.g., CePdAl, YbAgGe and UCoAl, which attract much attention due to the occurrence of a variety of metamagnetic transitions induced by geometrical frustration^{17,18} or a ferromagnetic QCP.¹⁹ Although local $4f$ electrons of Ce ions are coupled to conduction electrons below the Kondo temperature (~ 200 K), the magnetic susceptibility increases drastically upon cooling under a magnetic field H along the c axis.²⁰ This indicates that local moments are not fully screened even at low temperatures. Thereby, the magnetic susceptibility in $H \parallel c$ is roughly 30 times larger than that in $H \parallel a$. The reduced moments are approximately $0.05 \mu_B/\text{Ce}$ (μ_B is the Bohr magneton). The presence of antiferromagnetic interactions was suggested by the results of ¹¹⁹Sn-NMR experi-

ments on powder samples²¹ and by the negative values of the Curie-Weiss temperatures.²⁰ In zero field, however, no long-range magnetic order has been found at least above 50 mK.²² Instead, quantum critical phenomena were observed in the magnetic susceptibility, the electrical resistivity and the specific heat at low temperatures.²⁰

Recently, it was reported that QC in CeRhSn was fragile under a finite magnetic field;¹⁶ the non-Fermi-liquid (NFL) behavior in the low-temperature specific heat was rapidly suppressed with increasing field in any direction. This fact was attributed to the presence of a QCP near $H = 0$. Furthermore, the anisotropic temperature dependence of the thermal expansion α , showing a divergent behavior in α/T only along the a axis, suggests that QC is coupled to in-plane uniaxial pressure, which breaks the symmetry of the quasi-kagome lattice. By applying uniaxial pressure along the a axis, QC was indeed destroyed and complicated magnetic phase diagram was induced.²³ On the basis of these facts, CeRhSn has been considered a promising frustrated Kondo-lattice metal with a quantum spin-liquid ground state.^{16,24,25}

Another fascinating character of CeRhSn is the occurrence of a metamagnetic crossover under a magnetic field parallel to the a axis.^{16,26} Recently, a similar metamagnetic feature in $H \parallel a$ was reported for the isostructural CeIrSn as well.²⁷ In the previous report,¹⁶ the origin of this metamagnetic crossover was discussed in the analogy of the isostructural antiferromagnet YbAgGe, which exhibits spin-flop bicriticality under a magnetic field along the easy-magnetization plane ($\parallel ab$).¹⁸ It has been speculated that, due to the suppression of the magnetic-ordering temperature, the spin-flop metamagnetic transition becomes a crossover in CeRhSn.

As introduced above, the quasi-kagome Kondo-lattice CeRhSn exhibits various unusual properties, which are likely related to strong geometrical frustration of the reduced local $4f$ moments with Ising-like anisotropy. In the case of Ising-anisotropic materials, precise control of the magnetic-field orientation is essential to unravel the nature under a hard-axis magnetic field. It is because a tiny component of an easy-axis magnetic field may cause

dominant effect on its physical properties, as reported in Ising ferromagnets URhGe, UCoGe and UGe₂.^{28–30} For example, the gigantic upper critical field H_{c2} of a ferromagnetic superconductor UCoGe seen in $H \parallel b$ is intensely suppressed by tilting the magnetic field toward the easy c axis.³⁰ In this study, to take a closer look at the strange metallic state in CeRhSn, we performed field-angle-resolved measurements of its specific heat C , entropy S and magnetization M at low temperatures.

Results

Magnetization measurements. To obtain direct information on the magnetic property of CeRhSn under an exact in-plane magnetic field, dc magnetization was measured by using a home-made capacitively-detected Faraday magnetometer³¹ combined with the two-axis rotation device.³² The angle between the magnetic field and the ab plane, ϕ_H , was carefully determined within an error of better than 1° from magnetic-torque measurements by using the same setup (see Supplementary Fig. S1). Symbols in Fig. 1a show the magnetization curve, $M(H)$, measured at 0.15 and 4.2 K for $\phi_H = 0^\circ$. At 0.15 K, $M(H)$ shows an abrupt increase around $\mu_0 H_m \sim 3$ T, providing direct evidence for the occurrence of a metamagnetic crossover. By increasing temperature up to 4.2 K, $M(H)$ shows only a paramagnetic contribution; the metamagnetic crossover disappears in this field range. At 4.2 K, the $M(H)$ curve was also measured by using a commercial SQUID magnetometer (MPMS) and is represented by a solid line in Fig. 1a. The excellent agreement between the $M(H)$ curves taken with different instruments ensures high reliability of our magnetization data.

It is noted that the $M(H)$ curves at 0.15 and 4.2 K are roughly the same up to 2 T, reminiscent of the FL nature. In fact, $M(T)$ at 2 T in $H \parallel a$ does not depend on temperature below 2 K (inset of Fig. 1a). When H is tilted away from the ab plane by 5° , H_m increases slightly, and the low-field $M(H)$ is enhanced. The former can be more clearly seen in the field derivative of the magnetization, i.e., dM/dB (Fig. 1b). The latter can be attributed to the c -axis component of magnetization.

Thermal measurements. To apply the magnetic field exactly parallel to the ab plane, the field-angle ϕ_H dependence of the specific heat C was investigated at 0.1 K by rotating a magnetic field of 2 T within the ac plane. As shown in Fig. 2a, a sharp peak was observed in the $C(\phi_H)/T$ data centered at $\phi_H = 0^\circ$. Nearly the same ϕ_H dependence of the specific heat was obtained from a measurement in a rotating field within the a^*c plane, perpendicular to the a axis. These results indicate that the enhancement of the specific heat under an in-plane magnetic field can be easily destroyed by field misalignment of only a few degrees.

To provide further evidence for the anomalous state under a precisely-aligned in-plane magnetic field, a rela-

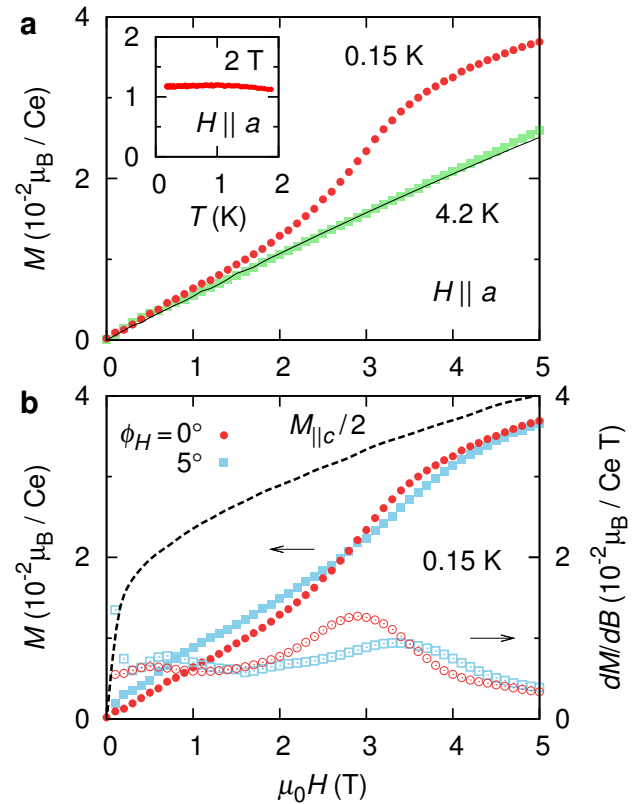


Figure 1: Magnetization process of CeRhSn with a fine-tuned field orientation. **a**, Field dependence of the magnetization $M(H)$ at 0.15 (circles) and 4.2 K (squares) in the exact in-plane direction. The solid line represents $M(H)$ at 4.2 K measured by MPMS in the approximate in-plane direction. Inset: $M(T)$ at 2 T in $H \parallel a$. **b**, $M(H)$ at 0.15 K for $\phi_H = 0^\circ$ (closed circles) and 5° (closed squares). Open symbols represent the field derivative of the magnetization. The dashed line shows the previously reported $M(H)$ curve at 0.5 K in $H \parallel c$,²⁰ which is divided in half.

tive change in the entropy S with ϕ_H was investigated via the field-rotational technique.¹⁵ Figure 2b shows the field-rotational magnetocaloric effect at 0.1 K in 2 T within the ac plane. By using the thermodynamic relation, $(\partial S/\partial \phi_H)_{T,H} = -C/T(\partial T/\partial \phi_H)_{S,H}$, the relative change in S with ϕ_H , $\Delta S_\phi = S(\phi_H) - S(90^\circ)$, was investigated and plotted in Fig. 2c. ΔS_ϕ shows a very sharp peak at $\phi_H = 0^\circ$ with a full width at half maximum of at most 4° (inset of Fig. 2c). This is evidence that QC is robust against H exactly parallel to the quasi-kagome plane.

However, when the in-plane field exceeds approximately 3 T, the high-entropy state is destroyed abruptly. Figures 3a and 3b show the field variations of C/T and the entropy change $\Delta S_H = S(H) - S(0)$ at 0.1 K, respectively. The latter is evaluated by using the relation $(\partial S/\partial H)_{T,\phi_H} = -C/T(\partial T/\partial H)_{S,\phi_H}$, i.e., the conventional field-sweep magnetocaloric effect. In $H \parallel a$, the entropy is gradually released at low fields below roughly

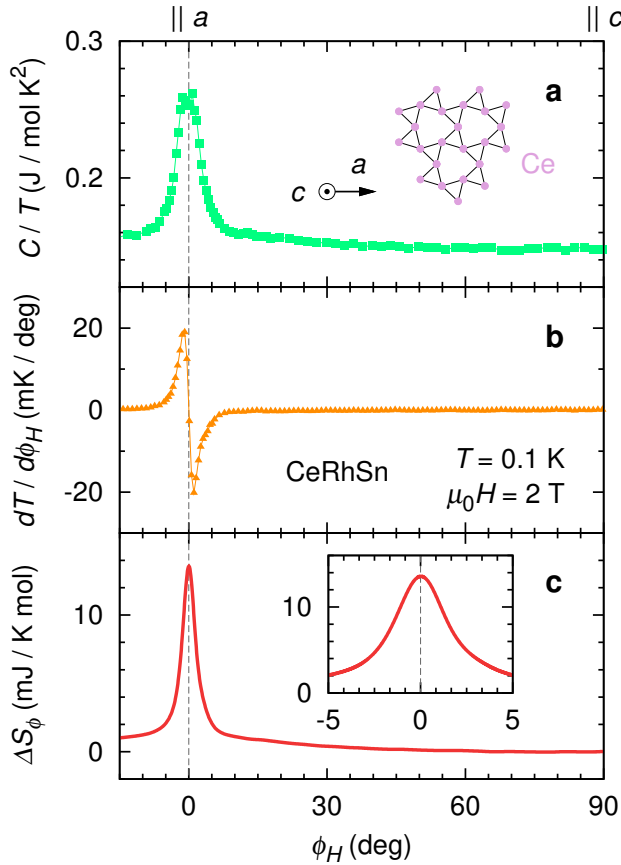


Figure 2: Field-angle dependence of thermodynamic quantities for CeRhSn. **a–c**, C/T (**a**), field-rotational magnetocaloric effect (**b**) and relative entropy change ΔS_ϕ (**c**) as a function of ϕ_H at 0.1 K. Here, the applied magnetic field of 2 T is rotated within the ac plane. Inset in **a**: top view along the c axis of the quasi-kagome lattice formed by Ce atoms in CeRhSn. Inset in **c**: enlarged plot of ΔS_ϕ near $\phi_H = 0^\circ$.

1 T and decreases remarkably at $\mu_0 H_m \sim 3$ T (Fig. **3b**). Around H_m , $C(H)/T$ shows an anomalous peak (Fig. **3a**), similar to the one observed in the previous report.¹⁶ The entropy plateau in 1–2 T suggests the formation of novel ground states under the in-plane magnetic field.

Figures **4a** and **4b** show the temperature dependence of C/T at various fields for $\phi_H = 0^\circ$ and 90° , respectively. The NFL behavior, i.e., increase of $C(T)/T$ on cooling, can be clearly seen in zero field. Under an in-plane magnetic field of larger than 4 T (above H_m) or fields along the c axis, the low-temperature $C(T)/T$ is nearly independent of temperature and likely in the FL regime; a weak upturn originates from the nuclear contribution. In sharp contrast to the previous observation of the strong suppression in $C(T)/T$ under 2 T,¹⁶ the NFL behavior remains at least up to 2 T for $H \parallel a$. In this NFL regime, the low-temperature $C(T)/T$ can be fitted well using a power-law function, $f(T) = \alpha T^{-n} + \gamma_0$. The parameters obtained by the fits are summarized in Table 1. With

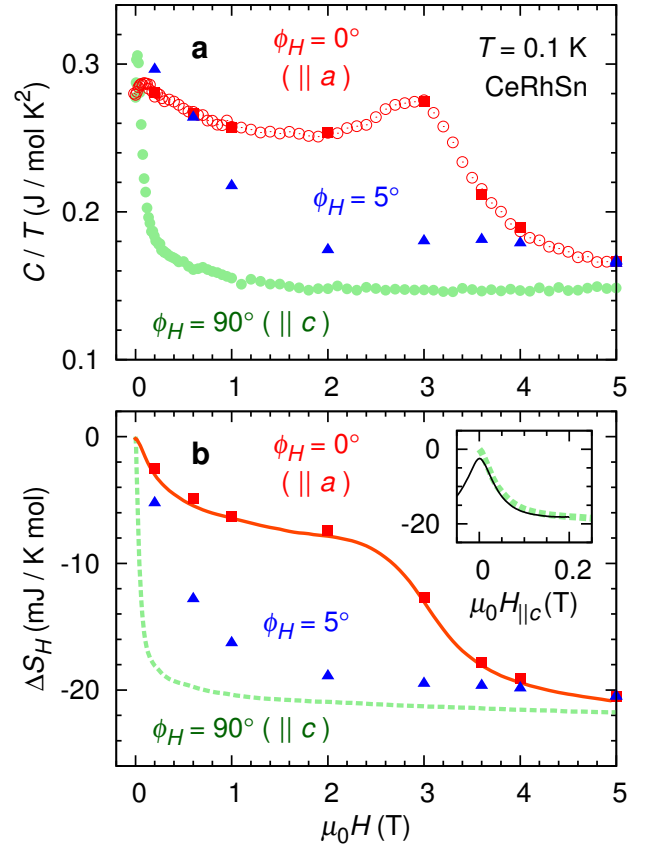


Figure 3: Magnetic field dependence of thermodynamic quantities of CeRhSn. **a**, **b**, Field dependence of $C(H)/T$ (**a**) and ΔS_H (**b**) at 0.1 K for $\phi_H = 0^\circ$ and 90° . The solid squares and triangles in **a** (**b**) are the field-rotational $C(\phi_H)/T$ [$\Delta S(H, \phi_H)$ (see Methods for details)] data at $\phi_H = 0^\circ$ and 5° , respectively. Inset in **b**: $\Delta S_H(H, 90^\circ)$ (dashed line) and $\Delta S(0.2 \text{ T}, \phi_H)$ (solid line) at 0.1 K as a function of $H_{\parallel c}$.

increasing H from 0 to 1 T, the exponent n changes drastically from $n \approx 1.5$ to $n \approx 1.0$. However, it is nearly unchanged in the entropy-plateau regime ($n \approx 1.0$ for $1 \text{ T} \leq \mu_0 H \leq 2 \text{ T}$). For $\mu_0 H \geq 3 \text{ T}$, the fit with $n \approx 1.0$ is not successful because of the breakdown of the NFL state.

One may suspect that the NFL behavior in $C(T)/T$ is incompatible with the FL-like behavior in $M(T)$ for $H \parallel a$. However, the plateau in $C(H)/T$ around 2 T (Fig. **3a**) is consistent with the temperature-independent magnetization (inset of Fig. **1a**), satisfying the thermodynamic Maxwell relation $\partial(C/T)/\partial H = \partial^2 M/\partial T^2$. These contrasting temperature responses of $M(T)$ and $C(T)/T$, similar to the recent observations in Ni-doped CeCoIn₅,³³ indicate that QC is coupled to spin fluctuations along the c axis, which do not affect the in-plane magnetization directly.

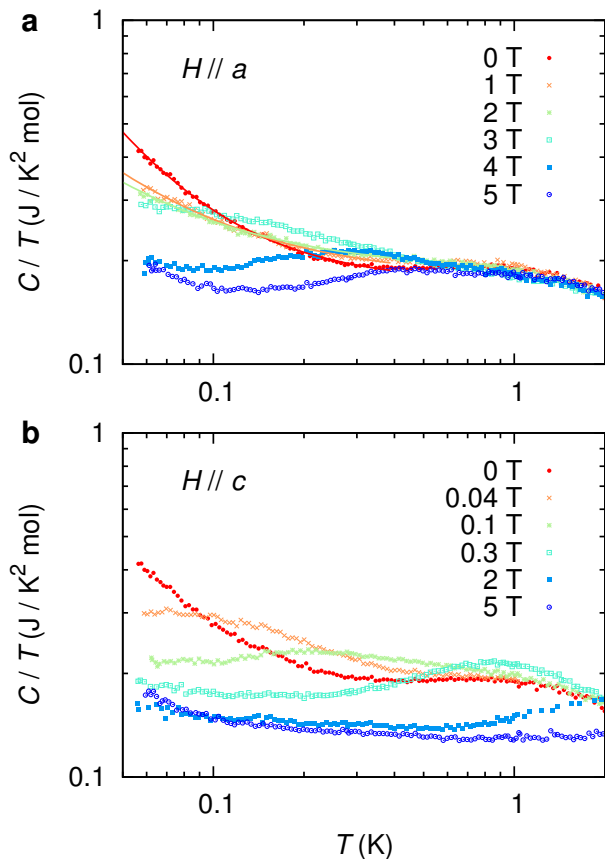


Figure 4: Quantum critical behaviors in C/T . **a, b,** Temperature dependence of C/T at $\phi_H = 0^\circ$ (**a**; $H \parallel a$) and $\phi_H = 90^\circ$ (**b**; $H \parallel c$). Solid lines in **a** represent the fits to the data at 0, 1 and 2 T using a function $f(T) = \alpha T^{-n} + \gamma_0$. The fitting parameters are shown in Table 1.

Table 1: Parameters obtained by the power-law fits to the specific-heat data. The $C(T)/T$ data for $H \parallel a$ were fitted using a power-law function $f(T) = \alpha T^{-n} + \gamma_0$. The fitting range is $T \leq 0.4$ K.

$\mu_0 H_{\parallel a}$ (T)	n	α (mJ/mol K $^{2+n}$)	γ_0 (J/mol K 2)
0	1.48	3.56	0.173
1	1.08	7.21	0.177
2	1.04	6.75	0.186

Field-angle-resolved mapping of thermodynamic quantities. Figures 5a–5c represent the contour maps of C , $dT/d\phi_H$ and $\Delta S [= S(H, \phi_H) - S(H = 0)]$ in the H – ϕ_H plane at 0.1 K, which were constructed via field-rotational measurements. The data points at $\phi = 0^\circ$ extracted from Figs. 5a and 5c are plotted in Figs. 3a and 3b as squares for comparison with the data taken

via field-sweep measurements drawn as open circles and a solid line, respectively. Good agreement between them further assures the reliability of our measurements. Figure 5d summarizes the phase diagram in the T – $H_{\parallel a}$ – $H_{\parallel c}$ space, where $H_{\parallel a} = H \cos \phi_H$ and $H_{\parallel c} = H \sin \phi_H$. The high-entropy state arises in the narrow angle range for $|\phi_H| \lesssim 2^\circ$ until H reaches H_m or $H_{\parallel c}$ exceeds a critical value. It should be emphasized that, with increasing H , the low-temperature entropy is stepwisely (monotonically) released at $\phi_H = 0^\circ$ ($\phi_H = 90^\circ$) and becomes nearly isotropic above H_m . The extrapolation of the entropy landscape to the $H_{\parallel a}$ – $H_{\parallel c}$ plane at 0 K demonstrates the existence of a quantum critical line at $H_{\parallel c} = 0$ and $|\mu_0 H_{\parallel a}| \lesssim 2.5$ T.

At $\phi_H = 5^\circ$, $S(H)$ decreases rapidly with increasing H (triangles in Fig. 3b), well below H_m (see Fig. 1b). This means that QC is more easily destroyed by $H_{\parallel c}$. For $H \parallel c$, QC is sensitively suppressed at very low fields below 0.1 T. This monotonic and rapid decrease of the entropy by $H_{\parallel c}$ can also be confirmed from the ΔS_ϕ data in low fields (solid line in the inset of Fig. 3b). The good match between the solid and dashed lines in the inset of Fig. 3b demonstrates that $H_{\parallel c}$ is a main origin for the suppression of QC.

Discussion

Let us discuss the possible mechanisms of QC in CeRhSn. Key features found in this study are as follows. First, QC is destroyed by the application of $H_{\parallel c}$ or the occurrence of a metamagnetic crossover. Second, QC is decoupled from the magnetization along the a axis. Third, the low-temperature entropy is stepwisely (monotonically) released in $H \parallel ab$ ($H \parallel c$) and becomes nearly isotropic above H_m . Fourth, the NFL behavior in $C(T)/T$ changes qualitatively under $H_{\parallel a}$ below 1 T and it becomes invariant in the entropy-plateau regime. These findings clearly support that spin fluctuations along the c axis are the main driving force for QC in CeRhSn; at the metamagnetic crossover, the spin fluctuations would be strongly suppressed.

The ultra-sensitive response of QC against ϕ_H is reminiscent of the steep field-angle dependence of H_{c2} in UCoGe;^{30,34} the angle-resolved NMR measurements on UCoGe revealed the intimate relation between its gigantic H_{c2} and ferromagnetic fluctuations along the c axis,³⁴ both which are strongly suppressed by $H_{\parallel c}$. This similarity apparently suggests that the key spin fluctuations for QC in CeRhSn are of the ferromagnetic type. This scenario is, however, inconsistent with various experimental facts supporting the frustration scenario,^{16,23} in which antiferromagnetic interactions play an essential role. The c -axis spin fluctuations caused by magnetic frustration would be easily coupled to $H_{\parallel c}$. Further studies are necessary to resolve this puzzle, e.g., from NMR measurements under a precisely aligned in-plane magnetic field.

In general, QC develops only near a QCP. In CeRhSn,

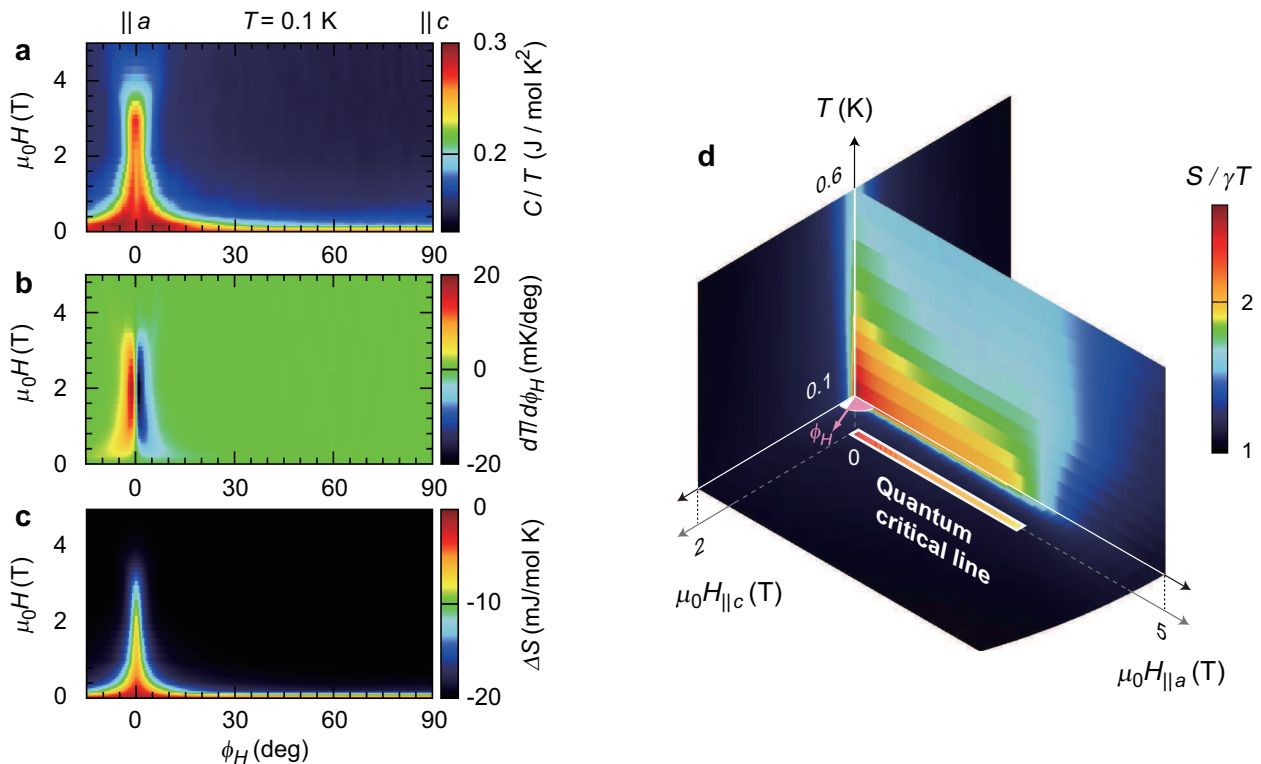


Figure 5: Landscape of quantum criticality in CeRhSn. **a–c**, Contour plots of C/T (**a**), $dT/d\phi_H$ (**b**) and ΔS (**c**) in the H - ϕ_H plane at 0.1 K. **d**, Entropy landscape in the T - $H_{||a}$ - $H_{||c}$ space, where $S/\gamma T$ is depicted using color on three selected planes for $T \geq 0.1$ K. Here, the Sommerfeld coefficient $\gamma = 132$ mJ/(mol K²) is adopted. A quantum critical line at $H_{||c} = 0$ and $|\mu_0 H_{||a}| \lesssim 2.5$ T is represented by a thick line outlined in white. See also Supplementary Figs. **S2** and **S3**.

however, QC survives over a wide range of tuning parameter $H_{||a}$ values. This QC feature resembles the enigmatic quantum critical “phases” proposed for β -YbAlB₄ and MnSi^{11,12,35} in which QC was observed in a wide range of hydrostatic pressures, even far away from the phase boundary of the magnetic order. Therefore, QC in CeRhSn is not associated with a conventional magnetic QCP. Moreover, in the T - $H_{||a}$ map in Fig. 5d, there are strong and weak quantum critical regimes, separated around $\mu_0 H_{||a} \sim 0.5$ T. The qualitative change in QC is also indicated by the low-temperature part of $C(T)/T$ (Fig. 4a), whose power-law temperature exponent n changes significantly between 0 and 1 T (Table 1). Around this characteristic field ($\mu_0 H_{||a} \sim 0.5$ T), a magnetic phase transition is induced by in-plane stress,²³ supporting a possible change in ground states. More importantly, the entropy plateau (Fig. 3b) along with the perfect match between the exponents n of $C(T)/T$ in 1–2 T (Fig. 4a and Table 1) emphasizes the emergence of a quantum critical “phase” driven by the precisely aligned in-plane magnetic field. These features capture new aspects of QC caused by unconventional origins. For CeRhSn, partially frustrated ground states transformed from the zero-field highly frustrated ones may stabilize the observed quantum critical “phase”. For compari-

son, a similar entropy plateau was reported on pyrochlore compounds,³⁶ which is attributable to the occurrence of the partially frustrated kagome-ice state under H along the cubic $\langle 111 \rangle$ axis, transformed from the fully frustrated spin-ice state in zero field.

Our multidimensional entropy landscape reveals various uncommon features of QC in CeRhSn. Particularly, the observation of QC in the very narrow field-angle range, $|\phi_H| \lesssim 2^\circ$, demonstrates that a magnetic field angle can be a powerful tuning parameter for QC. The field-angle-resolved entropy landscape, which directly reflects the degeneracy of ground states, has a great potential to advance our understanding of exotic phases in anisotropic systems. In particular, this technique opens a new route for the study of frustrated systems, such as magnetic monopole excitations,³⁷ a variety of spin-liquid states^{25,38,39} and field-induced novel phases, in which macroscopic degeneracy of ground states led by geometrical frustration plays a significant role.

Methods

Single-crystal growth. Single crystals of CeRhSn were grown by the Czochralski method using an rf induction

furnace.²⁰ A single piece with a weight of 44.0 mg mass was used in this study. It was cut into a thin slab, whose dimensions were roughly 3 mm \times 3 mm \times 0.2 mm along the a , c and a^* axes, respectively.

Magnetization measurements. The dc magnetization was measured using a home-built capacitively detected Faraday magnetometer³¹ combined with a two-axis alignment device,³² which was installed in a dilution refrigerator (Kelvinox MX100, Oxford). The magnetic field was generated along the vertical z direction using a solenoid magnet equipped with a gradient coil producing the field gradient in the z direction (dH_z/dz). The field gradient of 1 (5) T/m was used for the measurement at 0.15 (4.2) K. The sample was mounted on the capacitor transducer so that the a (c) axis was oriented close to the z (x) direction. The angle between the field and the ab plane ϕ_H was tuned by rotating the magnetometer around the y axis using a home-made tilting stage. A magnetic force F proportional to the sample magnetization, $F = MdH/dz$, in addition to the magnetic-torque background, was detected as a capacitance change of the capacitor transducer. The magnetic-torque component was measured separately under a zero field gradient $dH_z/dz = 0$, and its contribution was subtracted from the data. In the magnetization measurements, $\phi_H = 0^\circ$ was defined as the angle at which the magnetic-torque component is almost eliminated (Supplementary Fig. S1). For comparison, the magnetization was also measured using a commercial SQUID magnetometer (MPMS, Quantum Design).

Thermal measurements. The specific heat and the field-rotational magnetocaloric effect were measured by the quasi-adiabatic technique using a home-built calorimeter.¹⁵ The field-rotational magnetocaloric effect is the observed temperature change in response to the adiabatic rotation of the external magnetic field, which was investigated by fitting the initial slope of the temperature change, $dT/d\phi_H$, during each field rotation by 1° or 0.5° . Using the thermodynamic relation, $(\partial S/\partial\phi_H)_{T,H} = -C/T(\partial T/\partial\phi_H)_{S,H}$, the relative entropy change, $\Delta S_\phi(H, \phi_H) = S(H, \phi_H) - S(H, 90^\circ)$, can be evaluated as $\Delta S_\phi = -\int_{90^\circ}^{\phi_H} C/T(dT/d\phi_H)d\phi_H$. Likewise, the field variance of the entropy $\Delta S_H(H, \phi_H) = S(H, \phi_H) - S(H = 0)$ was evaluated as $\Delta S_H = -\int_0^H C/T(dT/dH)dH$ using the relation $(\partial S/\partial H)_{T,\phi_H} = -C/T(\partial T/\partial H)_{S,\phi_H}$, i.e., the conventional field-sweep magnetocaloric effect. In these thermal measurements, the sample was mounted on addenda of the calorimeter

so that the a^* axis was oriented along the z direction. It was cooled in a dilution refrigerator (Kelvinox AST Minisorb, Oxford) whose base temperature was well below 60 mK. The magnetic field was generated in the horizontal x direction up to 5 T using a split-pair magnet. By rotating the refrigerator around the z axis ($\parallel a^*$) using a stepper motor, the magnetic field was rotated on the ac plane.

Calibration of the entropy value. The ΔS_ϕ data at different H were compared by adding an offset of $\Delta S_H(H, 90^\circ)$ for each curve. In this way, we obtained the entropy change relative to $S(H = 0)$, i.e., $\Delta S_\phi(H, \phi_H) + \Delta S_H(H, 90^\circ) = S(H, \phi_H) - S(H = 0)$, which is referred to here as $\Delta S(H, \phi_H)$. Using $S = \gamma T$ and $\Delta S_H = 21.5$ mJ/(mol K) at 0.1 K in 5 T for $H \parallel c$, the absolute value of S was calibrated in the overall T - $H_{\parallel a}$ - $H_{\parallel c}$ space.

Data availability

The data that support the results of this study are available from the corresponding author on reasonable request.

Acknowledgments

We acknowledge helpful discussions with H. Tsunetsugu. This work has partially been supported by a Grant-in-Aid for Scientific Research on Innovative Areas ‘‘J-Physics’’ (JP15H05883, JP16H01076, JP18H04306) from MEXT, and JSPS KAKENHI Numbers JP17K05545, JP18H01161 and JP18H01164.

Author contributions

S.K. initiated the project. S.T. and T.T. synthesized the CeRhSn single crystal. S.K. performed the thermal measurements. S.K. Y.K. and T.S. performed the magnetization measurements. S.K. analyzed the data. S.K. and T.S. wrote the manuscript with input from all co-authors.

Competing interests

The authors declare no competing financial interests.

* kittaka@issp.u-tokyo.ac.jp

¹ Schröder, A. *et al.* Onset of antiferromagnetism in heavy-fermion metals. *Nature* **407**, 351 (2000).

² Si, Q., Rabello, S., Ingersent, K. & Smith, J. L. Locally critical quantum phase transitions in strongly correlated

metals. *Nature* **413**, 804 (2001).

³ Löhneysen, H. v., Rosch, A., Vojta, M. & Wölfle, P. Fermi-liquid instabilities at magnetic quantum phase transitions. *Rev. Mod. Phys.* **79**, 1015 (2007).

⁴ Gegenwart, P., Si, Q. & Steglich, F. Quantum criticality in

- heavy-fermion metals. *Nat. Phys.* **4**, 186 (2008).
- ⁵ Licciardello, S. *et al.* Electrical resistivity across a nematic quantum critical point. *Nature* **567**, 213 (2019).
 - ⁶ Michon, B. *et al.* Thermodynamic signatures of quantum criticality in cuprate superconductors. *Nature* **567**, 218 (2019).
 - ⁷ Custers, J. *et al.* The break-up of heavy electrons at a quantum critical point. *Nature* **424**, 524 (2003).
 - ⁸ Schuberth, E. *et al.* Emergence of superconductivity in the canonical heavy-electron metal YbRh₂Si₂. *Science* **351**, 485 (2016).
 - ⁹ Yuan, H. Q. *et al.* Observation of two distinct superconducting phases in CeCu₂Si₂. *Science* **302**, 2104 (2003).
 - ¹⁰ Tokiwa, Y., Ishikawa, J. J., Nakatsuji, S. & Gegenwart, P. Quantum criticality in a metallic spin liquid. *Nat. Mater.* **13**, 356 (2014).
 - ¹¹ Matsumoto, Y. *et al.* Quantum criticality without tuning in the mixed valence compound β -YbAlB₄. *Science* **331**, 316 (2011).
 - ¹² Tomita, T., Kuga, K., Uwatoko, Y., Coleman, P. & Nakatsuji, S. Strange metal without magnetic criticality. *Science* **349**, 506 (2015).
 - ¹³ Grube, K., Zaum, S., Stockert, O., Si, Q. & Löhneysen, H. v. Multidimensional entropy landscape of quantum criticality. *Nat. Phys.* **13**, 742 (2017).
 - ¹⁴ Rost, A. W., Perry, R. S., Mercure, J., Mackenzie, A. P. & Grigera, S. A. Entropy landscape of phase formation associated with quantum criticality in Sr₃Ru₂O₇. *Science* **325**, 1360 (2009).
 - ¹⁵ Kittaka, S., Nakamura, S., Kadowaki, H., Takatsu, H. & Sakakibara, T. Field-rotational magnetocaloric effect: a new experimental technique for accurate measurement of the anisotropic magnetic entropy. *J. Phys. Soc. Jpn.* **87**, 073401 (2018).
 - ¹⁶ Tokiwa, Y., Stingl, C., Kim, M. S., Takabatake, T. & Gegenwart, P. Characteristic signatures of quantum criticality driven by geometrical frustration. *Sci. Adv.* **1**, e1500001 (2015).
 - ¹⁷ Mochizuki, K. *et al.* Thermodynamic investigation of metamagnetic transitions and partial disorder in the quasikagome Kondo lattice CePdAl. *J. Phys. Soc. Jpn.* **86**, 034709 (2018).
 - ¹⁸ Tokiwa, Y., Garst, M., Gegenwart, P., Bud'ko, S. L. & Canfield, P. C. Quantum bicriticality in the heavy-fermion metamagnet YbAgGe. *Phys. Rev. Lett.* **111**, 116401 (2013).
 - ¹⁹ Aoki, D. *et al.* Ferromagnetic quantum critical endpoint in UCoAl. *J. Phys. Soc. Jpn.* **80**, 094711 (2011).
 - ²⁰ Kim, M. S. *et al.* Low-temperature anomalies in magnetic, transport, and thermal properties of single-crystal CeRhSn with valence fluctuations. *Phys. Rev. B* **68**, 054416 (2003).
 - ²¹ Tou, H., Kim, M. S., Takabatake, T. & Sera, M. Antiferromagnetic spin fluctuations in CeRhSn probed by ¹¹⁹Sn NMR. *Phys. Rev. B* **70**, 100407(R) (2004).
 - ²² Schenck, A., Gygax, F. N., Kim, M. S. & Takabatake, T. Study of the electronic properties of CeRhSn by μ^+ Knight shift and relaxation measurements in single crystals. *J. Phys. Soc. Jpn.* **73**, 3099 (2004).
 - ²³ Küchler, R. *et al.* Uniaxial stress tuning of geometrical frustration in a Kondo lattice. *Phys. Rev. B* **96**, 241110(R) (2017).
 - ²⁴ Vojta, M. Frustration and quantum criticality. *Rep. Prog. Phys.* **81**, 064501 (2018).
 - ²⁵ Balents, L. Spin liquids in frustrated magnets. *Nature* **464**, 199 (2010).
 - ²⁶ Yang, C. L. *et al.* Quantum criticality and development of antiferromagnetic order in the quasikagome kondo lattice CeRh_{1-x}Pd_xSn. *Phys. Rev. B* **96**, 045139 (2017).
 - ²⁷ Tsuda, S. *et al.* Metamagnetic crossover in the quasikagome Ising Kondo-lattice compound CeIrSn. *Phys. Rev. B* **98**, 155147 (2018).
 - ²⁸ Aoki, D., Ishida, K. & Flouquet, J. Review of U-based ferromagnetic superconductors: Comparison between UGe₂, URhGe, and UCoGe. *J. Phys. Soc. Jpn.* **88**, 022001 (2019).
 - ²⁹ Nakamura, S. *et al.* Wing structure in the phase diagram of the Ising ferromagnet URhGe close to its tricritical point investigated by angle-resolved magnetization measurements. *Phys. Rev. B* **96**, 094411 (2017).
 - ³⁰ Aoki, D. *et al.* Extremely large and anisotropic upper critical field and the ferromagnetic instability in UCoGe. *J. Phys. Soc. Jpn.* **78**, 113709 (2009).
 - ³¹ Farakibara, T., Mitamura, H., Tayama, T. & Amitsuka, H. Faraday force magnetometer for high-sensitivity magnetization measurements at very low temperatures and high fields. *Jpn. J. Appl. Phys.* **33**, 5067 (1994).
 - ³² Nakamura, S. *et al.* Low-temperature magnetization measurements with precise two-axis alignment of the sample orientation. *J. Phys. Soc. Jpn.* **87**, 114001 (2018).
 - ³³ Yokoyama, M. *et al.* Anisotropic magnetic-field response of quantum critical fluctuations in Ni-doped CeCoIn₅. *Phys. Rev. B* **99**, 054506 (2019).
 - ³⁴ Hattori, T. *et al.* Superconductivity induced by longitudinal ferromagnetic fluctuations in UCoGe. *Phys. Rev. Lett.* **108**, 066403 (2012).
 - ³⁵ Doiron-Leyraud, N. *et al.* Fermi-liquid breakdown in the paramagnetic phase of a pure metal. *Nature* **424**, 595 (2003).
 - ³⁶ Hiroi, Z., Matsuhira, K., Takagi, S., Tayama, T. & Sakakibara, T. Specific heat of kagomé ice in the pyrochlore oxide Dy₂Ti₂O₇. *J. Phys. Soc. Jpn.* **72**, 411 (2003).
 - ³⁷ Castelnovo, C., Moessner, R. & Sondhi, S. L. Magnetic monopoles in spin ice. *Nature* **451**, 42 (2008).
 - ³⁸ Gingras, M. J. P. & McClarty, P. A. Quantum spin ice: a search for gapless quantum spin liquids in pyrochlore magnets. *Rep. Prog. Phys.* **77**, 056501 (2014).
 - ³⁹ Savary, L. & Balents, L. Quantum spin liquids: a review. *Rep. Prog. Phys.* **80**, 016502 (2017).

Thermodynamic evidence for novel quantum criticality in a frustrated metal

Shunichiro Kittaka,¹ Yohei Kono,¹ Suguru Tsuda,² Toshiro Takabatake,² Toshiro Sakakibara¹

¹ Institute for Solid State Physics, University of Tokyo, Kashiwa, Chiba 277-8581, Japan

² Department of Quantum matter, AdSM, Hiroshima University, Higashi-Hiroshima 739-8530, Japan

Supplementary Information

Magnetization measurements

In this study, dc magnetization was measured using a home-made capacitively detected Faraday magnetometer combined with a two-axis rotation device.³² The angle ϕ_H between H and the ab plane was controlled precisely by rotating the sample around the a^* axis using the tilting stage of the two-axis rotation device. The piezo-stepper-driven goniometer attached on the tilting stage was fixed so that the a^* axis was nearly parallel to the rotational axis of the tilting stage.

First, we carefully placed the field orientation exactly parallel to the ab plane via magnetic-torque measurements. Magnetic torque can be detected as a capacitance change of a capacitor transducer under a zero field gradient. Figure **S1a** shows the relative change in the raw capacitance data ΔC with H , measured under a zero field gradient for several ϕ_H values. By rotating the tilting stage, a large dip in $\Delta C(H)$ around $\mu_0 H \sim 3$ T, originating from the metamagnetic crossover, was suppressed and changed into a peak. This sign change of the magnetic-torque component in ΔC indicates that H crossed the ab plane. Therefore, we defined the angle at which $\Delta C(H)$ became nearly independent of H as $\phi_H = 0^\circ$ (dashed line in Fig. **S1a**). Owing to this fine-tuning, the magnetic field could be applied parallel to the ab plane with a high precision, better than 1° .

Then, using the same setup, we performed magnetization measurements. Figure **S1b** shows the magnetization curve $M(H)$ for $\phi_H = 1^\circ$ at 0.2 K, compared with $M(H)$ for $\phi_H = 0^\circ$ at 0.15 K. Above the metamagnetic-crossover field H_m , no anomaly was found up to 14 T. From this figure, it is evident that the $M(H)$ curve is not affected significantly by a possible tiny field misalignment less than 1° , as well as a slight difference in temperature.

Thermal measurements

The field-angle-resolved landscapes of the thermodynamic quantities shown in Figs. **5a–5c** were constructed using the data in Figs. **S2a–S2c**, respectively. As shown in Fig. **S2a**, the low-field $C(\phi_H)/T$ measured at a finite temperature of 0.1 K shows peaks at non-zero ϕ_H because of the development of a Schottky-type anomaly by applying $H_{\parallel c}$, which results in a prominent dip at $\phi_H = 0^\circ$. By contrast, $S(\phi_H)$ always shows a peak centered at $\phi_H = 0^\circ$, directly reflecting the high degeneracy of the ground states (Fig. **S2c**). Thus, entropy is more powerful to reveal the field-angle dependence of quantum criticality than specific heat.

According to the Maxwell relation, we obtain $(\partial S/\partial \phi_H)_{H,T} = (\partial \tau_\phi/\partial T)_{H,\phi_H}$, where τ_ϕ denotes the in-plane magnetic torque. By taking advantage of this relation, we can define symmetric crystalline axes along which H induces $\tau_\phi = 0$. For CeRhSn, $\phi_H = 0^\circ$ can be defined with high precision much better than 0.5° because the field-rotational magnetocaloric effect $dT/d\phi_H \propto (\partial \tau_\phi/\partial T)_{H,\phi_H}$ changes its sign sharply at $\phi_H = 0^\circ$ (Fig. **S2b**). It also gives a good indication of the angle range where the entropy changes drastically. The contour maps in Figs. **5a–5c** help us confirm these features more easily.

Figures **S3a** and **S3b** show the raw data of $S/\gamma T$, which were used for constructing the $T-H_{\parallel a}$ and $T-H_{\parallel c}$ landscapes in Fig. **5d**, respectively. Although $S/\gamma T$ decreases rapidly and monotonically in $H \parallel c$, it shows a two-step decrease in $H \parallel a$. The first, low-field decrease around 0.5 T is gradually smeared out with increasing temperature. The second decrease around 3 T shifts toward higher fields with increasing temperature, following the metamagnetic crossover field $H_m(T)$. Uncommonly, there is a wide field region, where $S/\gamma T$ is insensitive to a tuning parameter $H_{\parallel a}$, below H_m . This entropy plateau suggests the existence of a secondary quantum critical state, which is qualitatively different from the zero-field one.

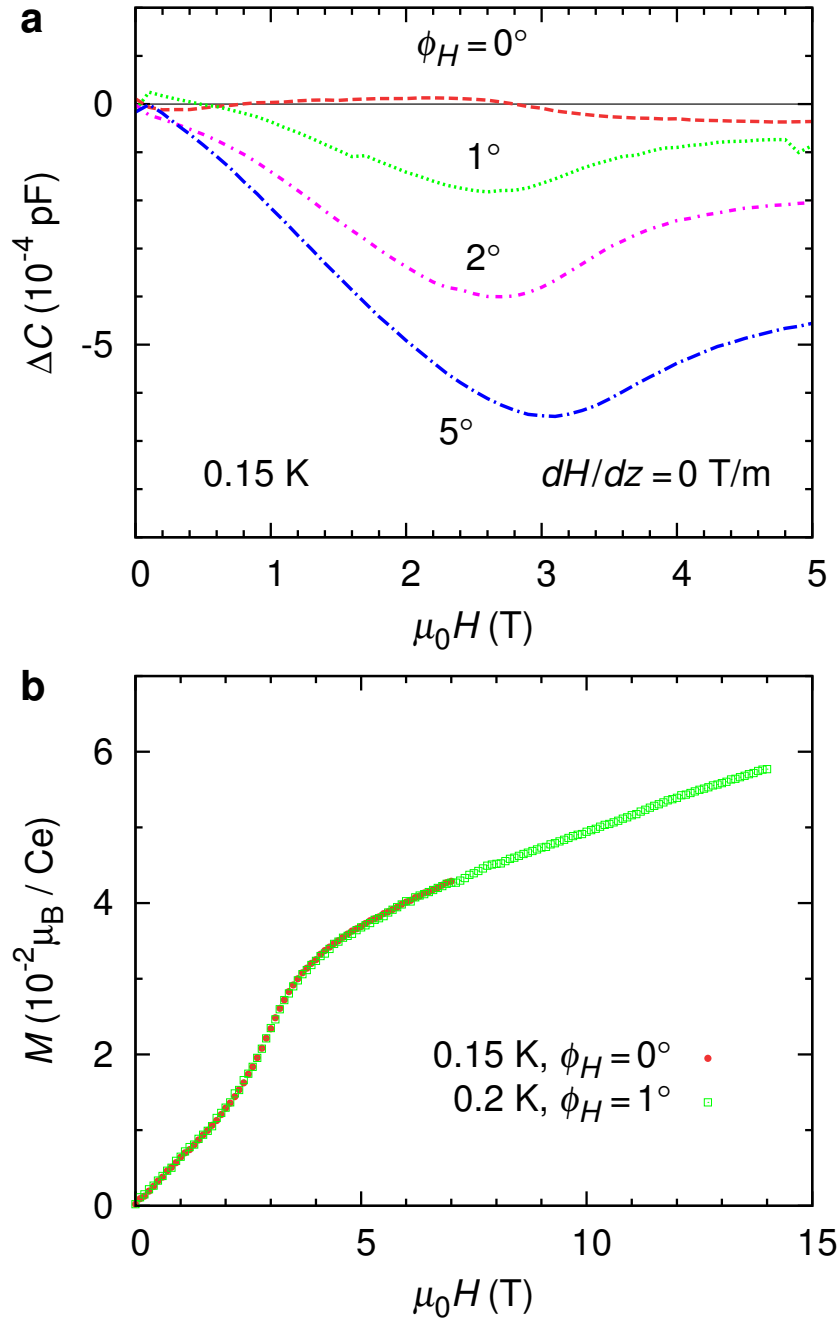


Figure S1: Field dependence of the magnetic-torque component and magnetization at several field angles. a, Relative change in the raw capacitance data, ΔC , measured with a zero field gradient at 0.15 K for several ϕ_H . The solid line is the zero-torque state. **b,** The magnetization curve $M(H)$ for $\phi_H = 1^\circ$ up to 14 T measured at 0.2 K, compared with $M(H)$ for $\phi_H = 0^\circ$ measured at 0.15 K.

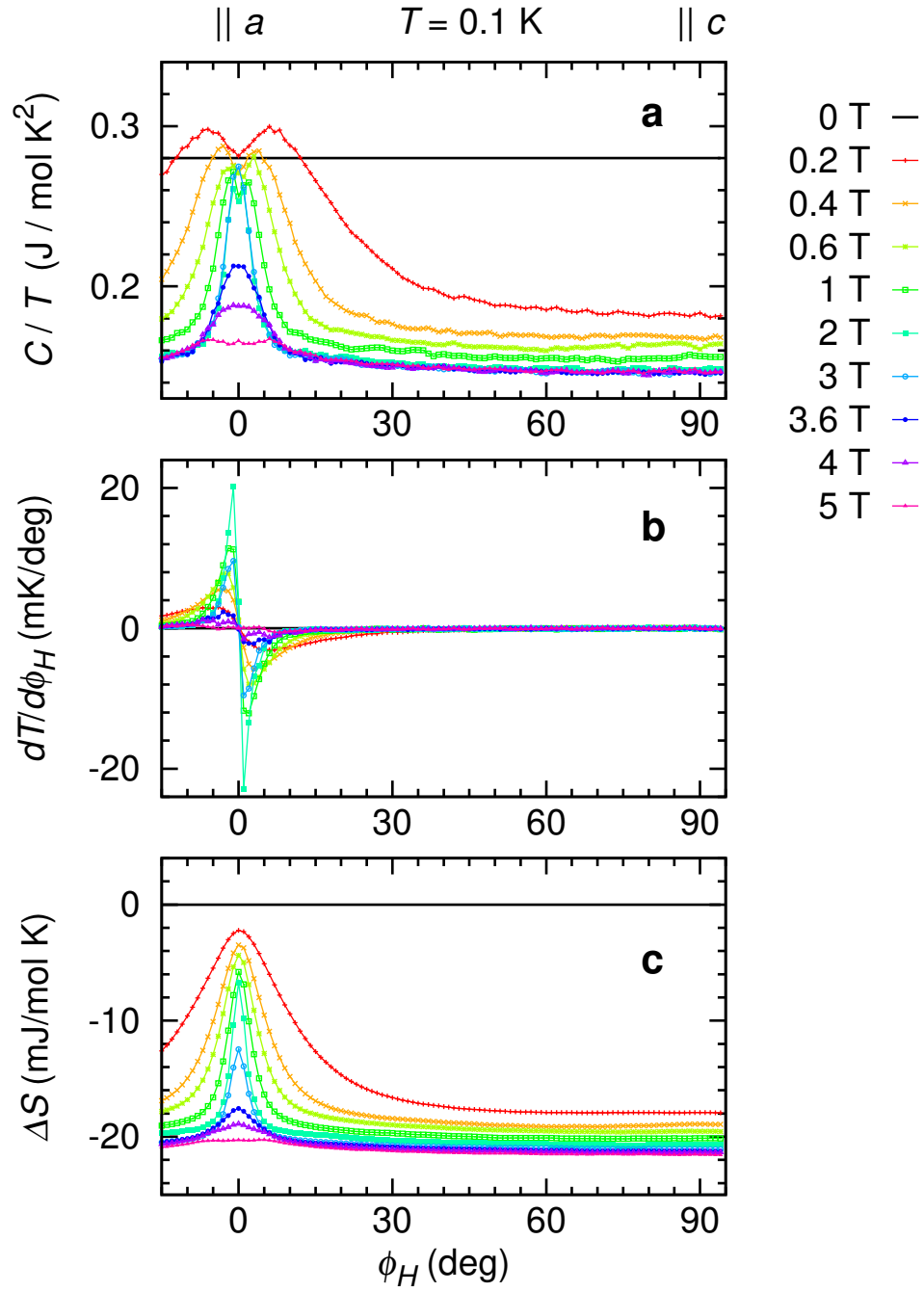


Figure S2: Raw data for constructing the landscape of quantum criticality shown in Figs. 5a–5c. a–c, Field-angle ϕ_H dependence of specific heat $C(H, \phi_H)/T$ (a), rotational magnetocaloric effect $dT/d\phi_H(H, \phi_H)$ (b) and entropy change $\Delta S(H, \phi_H) = \Delta S_\phi(H, \phi_H) + \Delta S_H(H, 90^\circ) [= S(H, \phi_H) - S(H = 0)]$ (c) at 0.1 K.

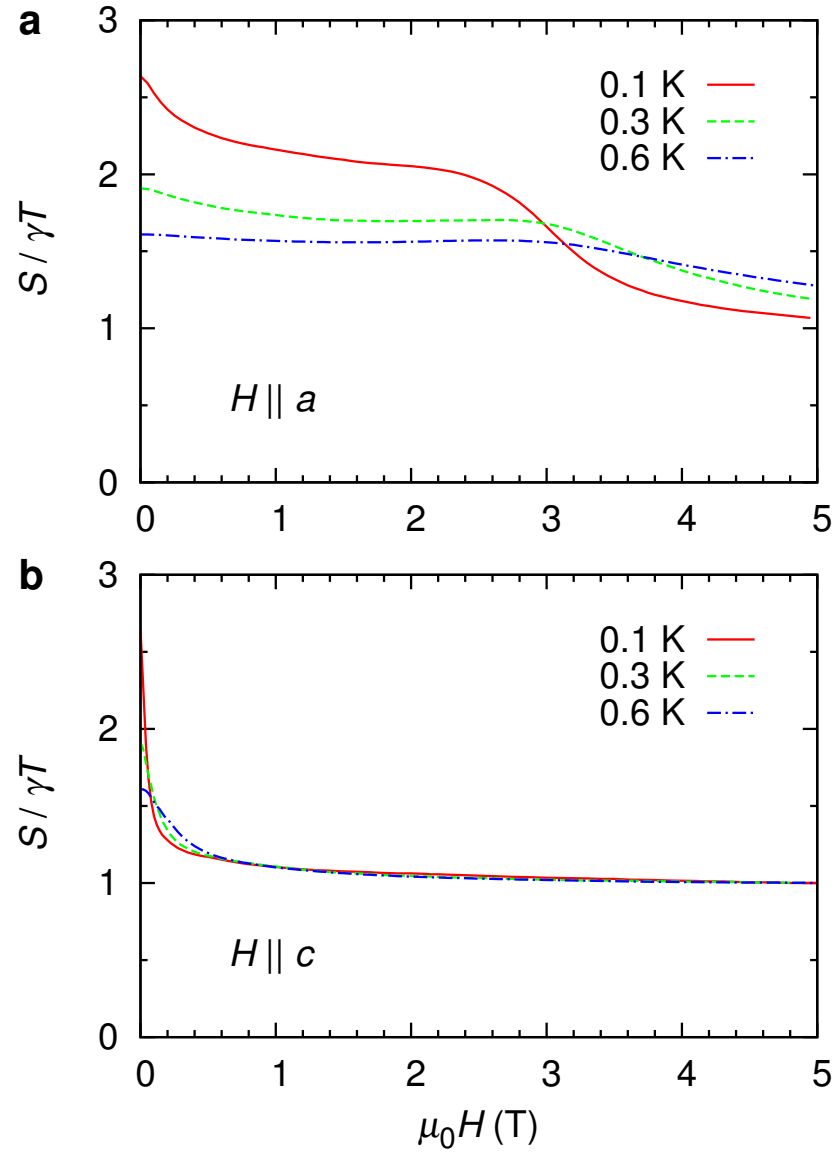


Figure S3: Raw data for constructing the landscape of quantum criticality shown in Fig. 5d. a, b, Field dependence of $S/\gamma T$ at $\phi_H = 0^\circ$ (a; $H \parallel a$) and $\phi_H = 90^\circ$ (b; $H \parallel c$).